atmosphere

MDPI

Supplementary Materials

Study of Methane Emission and Geological Sources in Northeast China Permafrost Area Under Engineering Construction and Climate Disturbance Based On Ground Monitoring and AIRS

Xu Zhichao [1,2,3,4,*], Chen Yunshan [5,6,*], Shan Wei [4], Deng Chao [1,2,3], Ma Min [1,2,3,4], Wu Yuexing [1,2], Mao Yu [1,2], Ding Xingyu [1,2] and Ji Jing [7,8]

1. Mean value of 400 hPa and 600 hPa troposphere methane concentration in China and Northeast China from 2003 to 2022.

The spatiotemporal distribution of methane concentration in the near-surface troposphere of China and Northeast China at different altitudes from 2003 to 2022 is shown in Figure 1 (400 hPa) and Figure 2 (600 hPa).

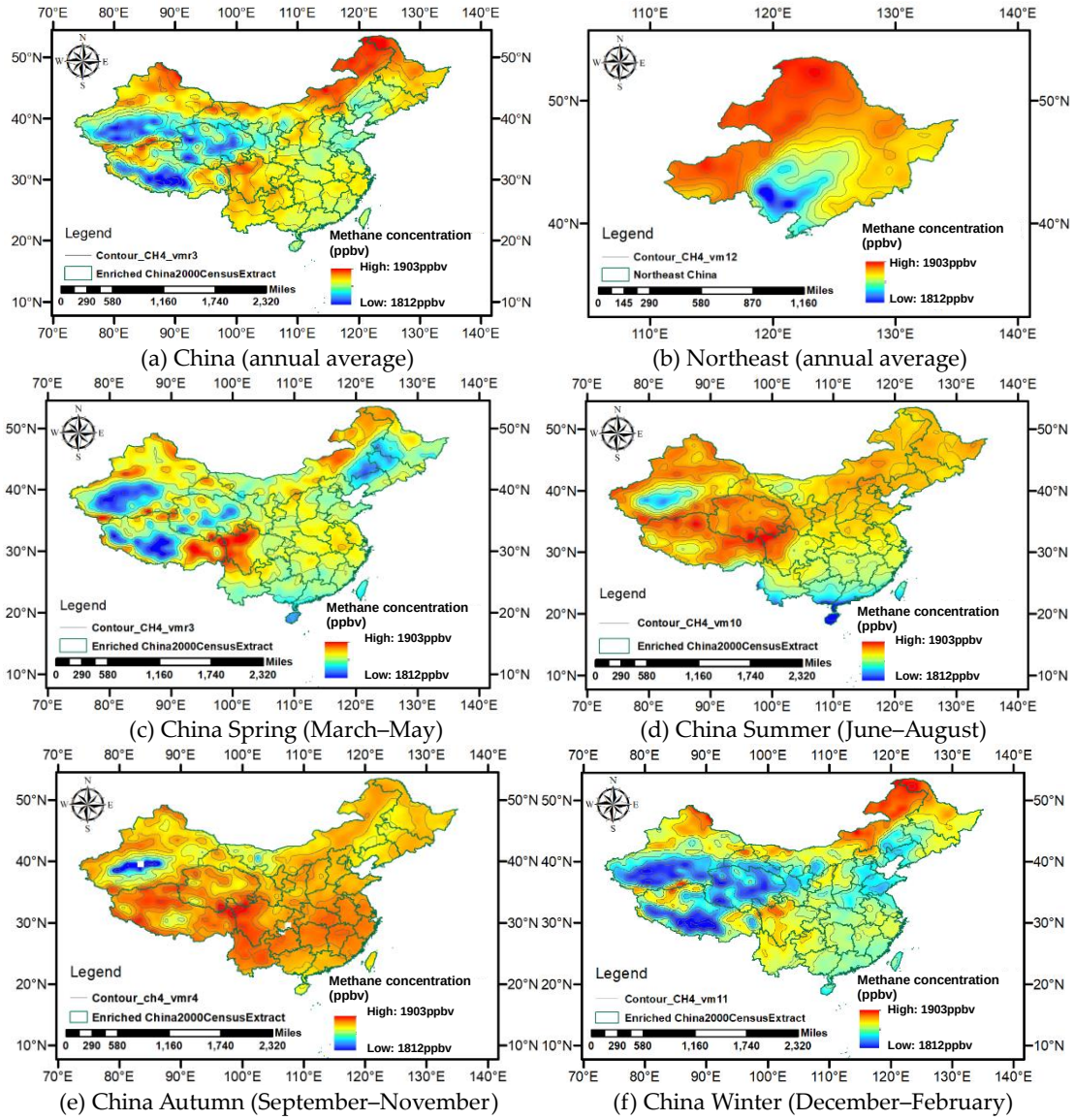

(a) China (annual average)

(b) Northeast (annual average)

(c) China Spring (March–May)

(d) China Summer (June–August)

(e) China Autumn (September–November)

(f) China Winter (December–February)

Figure S1. Mean value of 400 hPa troposphere methane concentration in China and Northeast China from 2003 to 2022.

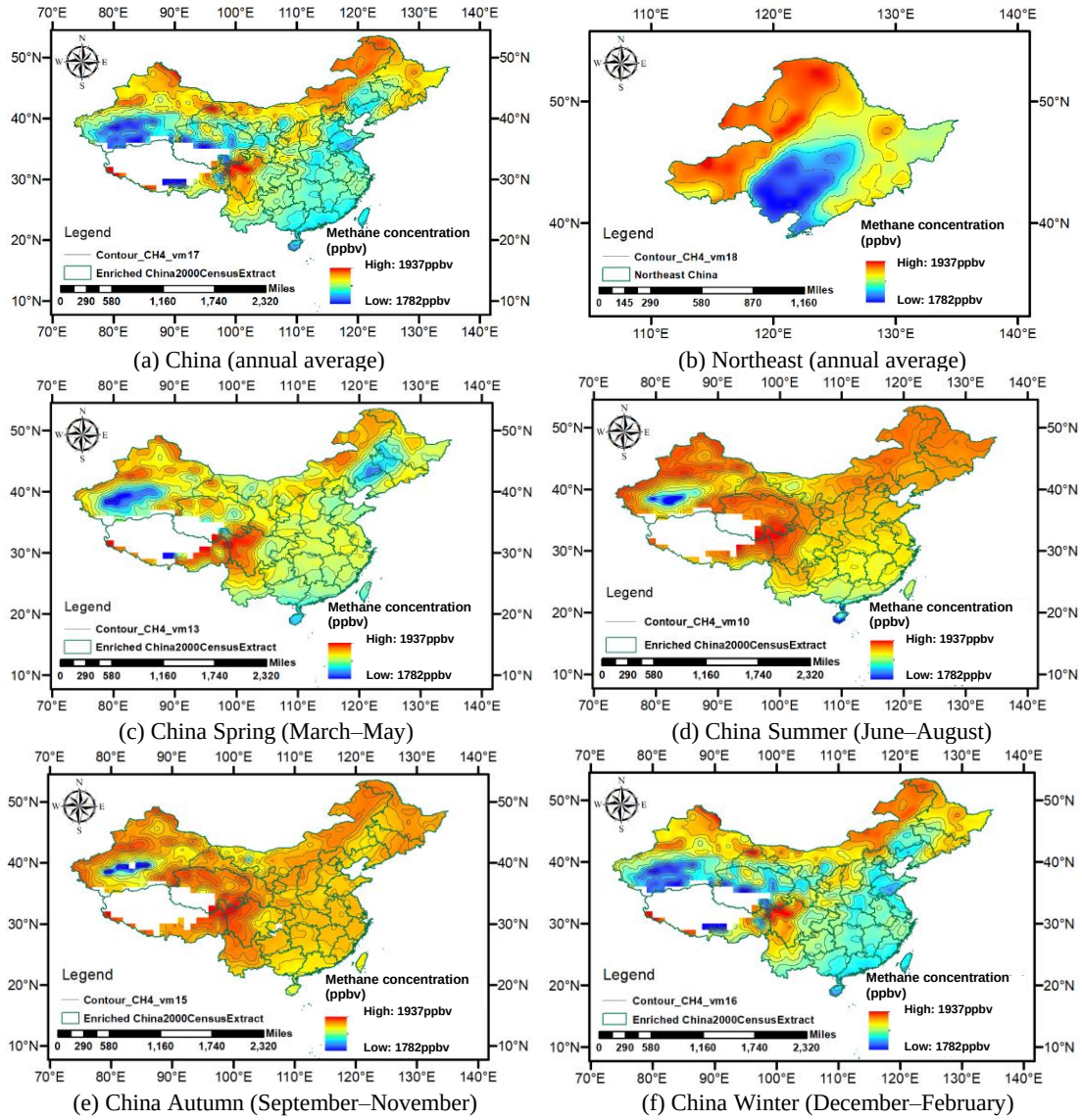

Figure S2. Mean value of 600 hPa troposphere methane concentration in China and Northeast China from 2003 to 2022.

2. Air methane concentration value of Waliguan (WLG)

To further compare the methane emission characteristics of the Northeast China permafrost area and the Qinghai–Tibet Plateau permafrost area, the methane concentration observation data of the Waliguan Global Atmospheric Background Station from 1992 to 2021 were analyzed (https://www.esrl.noaa.gov/gmd/dv/site/WLG.html). From the observation curve of air methane concentration in Waliguan area from 1992 to 2021 (Figure 10a), it can be seen that the air methane concentration in Waliguan showed an upward trend from 1992 to 2002 and was basically stable from 2002 to 2006. From 2007 to 2018, the overall growth was slow, the concentration of methane was the phased largest in 2018, and the annual average value of methane reached 1.9287 ppm. In 2019, it continued to grow, and grew faster.

In addition, it can be seen from the monthly mean value of air methane concentration in Waliguan that the air methane concentration in Waliguan is characterized by significant seasonal changes with two peaks (Figure 10a); the first peak occurs in summer (June–

August), and the maximum value occurs in August, at 1.8572 ppm. The second peak appears in winter (December–February), with the maximum value occurring in December, at 1.8461 ppm. Through comparative analysis of methane concentrations at observation point S-1 in the permafrost area of Northeast China in different seasons and depths, it was found that the maximum total methane emissions during the year occur in the summer, which is consistent with the observation results in the Waliguan. However, the maximum ground surface methane concentration at observation point S-1 occurs in spring, while the total amount and concentration of methane emissions in autumn and winter are relatively small. It is different from the Waliguan area.

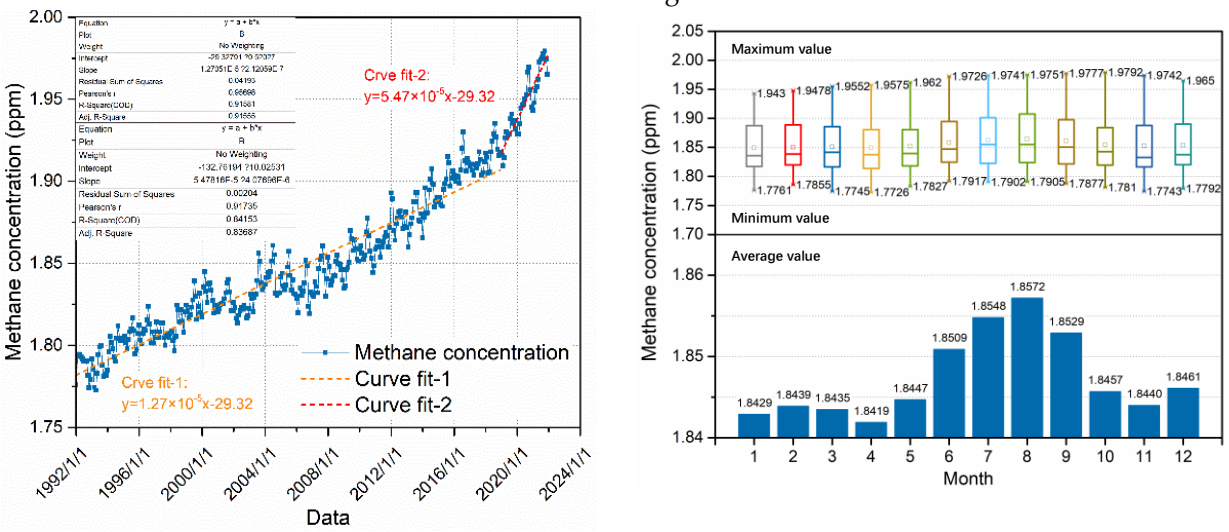

(a) Annual variation of methane concentration (b) Monthly variation of methane concentration

Figure S3. Air methane concentration value of Waliguan from 1992 to 2019. (a) Annual variation; (b) monthly variation. Each part of the box plot represents maximum, minimum, median, quartile, and outlier.

The manuscript introduces the methane emission characteristics of Waliguan, mainly comparing and analyzing the methane emission patterns in the high-latitude permafrost degradation areas of Northeast China and the high-altitude permafrost degradation areas of the Qinghai–Tibet Plateau. The reason for the difference between the two is related to geological structure and vegetation differences.

3. Geological methane leakage model

3.1. Equation of Methane clathrate decomposition

This paper uses the first-order kinetics proposed by Kim et al. as the control equation for the hydrate decomposition process：

$$R_h = n(s_h A_{hs} K_d \langle f_{eq} - f_g \rangle) \quad (1)$$

Among them, R_h is the rate of hydrate phase transition expressed in terms of the number of moles of hydrate, K_d is the kinetic constant of hydrate decomposition, A_{hs} is the surface area of hydrates per unit volume, f_g is the air pressure at a certain temperature, f_{eq} is the phase equilibrium pressure that depends on this temperature, and 〈〉 are Macaulay parentheses, the ramp function is described.

3.2. Equations of convective heat transfer in porous medium

Heat flows from the surface into the porous medium for transfer, and under the effect of the seepage field, heat gradually radiates to the hydrate layer containing methane and decomposes it.

Among them, ρ is the density, kg/m^3; C_P is the Specific heat capacity, J/(mol·K); Q is the heat source, in this paper, the heat absorbed by the methane hydrate reaction, W/m^3.

$$\begin{cases} \rho C_p \dfrac{\partial T}{\partial t} + \rho C_p \vec{u} \cdot \nabla T + \nabla \cdot \vec{q} = Q \\ \vec{u} = -\dfrac{\varphi}{\mu} \nabla p \\ \vec{q} = -\alpha_e \nabla T \end{cases} \tag{2}$$

In the equation: $\vec{u}$ is the velocity field under Darcy flow velocity, m/s; $\vec{q}$ is the heat conduction capacity, W/m^2; φ for permeability, m^2; μ is the dynamic viscosity, Pa·s; a_e is the thermal conductivity coefficient, W/(m·K). From this, it can be concluded that the energy consumption for hydrate decomposition is:

$$Q = m_h \Delta H \tag{3}$$

In the equation, ΔH is the decomposition heat of hydrates, with a value of 5158J/(kg·K).

3.3. Equation of methane gas migration in porous medium

$$\begin{aligned} &[\frac{\partial}{\partial x}(v_x c) + \frac{\partial}{\partial y}(v_y c) + \frac{\partial}{\partial z}(v_z c)] + [\frac{\partial}{\partial x}(nD_x \frac{\partial c}{\partial x}) + \frac{\partial}{\partial y}(nD_y \frac{\partial c}{\partial y}) + \frac{\partial}{\partial z}(nD_z \frac{\partial c}{\partial x})]\Delta x \Delta y \Delta z \\ &= \frac{\partial (nc)}{\partial t} \Delta x \Delta y \Delta z \end{aligned} \tag{4}$$

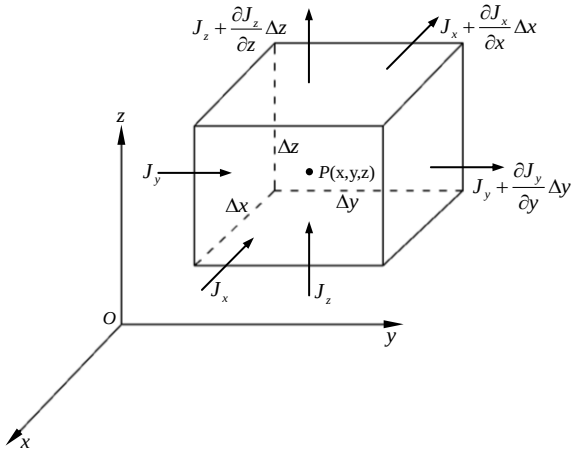

Figure S4. Hexahedron unit.

After sorting, it is found that the selected coordinate axis direction is consistent with the main seepage direction.

$$\frac{\partial (nc)}{\partial t} = \frac{\partial}{\partial x}(nD_x \frac{\partial c}{\partial x}) + \frac{\partial}{\partial y}(nD_y \frac{\partial c}{\partial y}) + \frac{\partial}{\partial z}(nD_z \frac{\partial c}{\partial z}) - [\frac{\partial}{\partial x}(v_x c) + \frac{\partial}{\partial y}(v_y c) + \frac{\partial}{\partial z}(v_z c)] \tag{5}$$

In the equation, *nc* is the mass of methane gas in the fluid in porous medium per unit of time and volume, $\frac{\partial (nc)}{\partial t}$ is the mass change of methane gas in the fluid in porous medium per unit of time and volume.

3.4. Equation of methane adsorption in porous medium

The convection–diffusion–adsorption equation of the saturated porous medium is:

$$\left\{1+\frac{(1-n)\rho_s}{n}K_d S_m[\frac{1}{1+K_d c}-\frac{K_d c}{(1+K_d c)^2}]\right\}\frac{\partial c}{\partial t}=\nabla\cdot(\boldsymbol{D}\cdot\nabla c-\boldsymbol{u}c) \quad (6)$$

$$R_d\frac{\partial c}{\partial t}=\nabla\cdot(\boldsymbol{D}\cdot\nabla c-\boldsymbol{u}c) \quad (7)$$

$$R_d=1+\frac{(1-n)\rho_s}{n}K_d S_m[\frac{1}{1+K_d c}-\frac{K_d c}{(1+K_d c)^2} \quad (8)$$

3.5. Basic parameters of the model

With the intensification of global warming, the permafrost layer gradually melts, and its protective effect on the low-temperature and high-pressure environment required for the stable existence of methane hydrate disappears, leading to the gradual decomposition of methane hydrate and the formation of a large number of methane gas after the external heat flow enters, and this part of methane gas will continue to migrate to the surface gradually under the pressure gradient and diffusion.

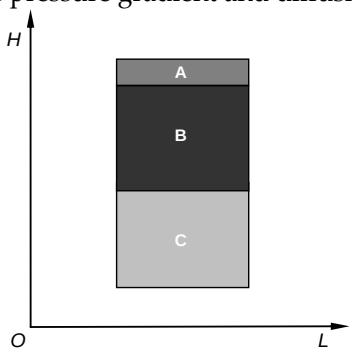

Figure S5. Simplified physical model.

The migration of methane gas in porous medium (such as soil, aquifer, etc.) is very complex, involving many factors, such as temperature, concentration, pH, plant absorption, microbial activity, porous medium heterogeneity, and anisotropy. Methane gas in a porous medium will also produce physical functions such as convection, diffusion, and dispersion, as well as chemical functions such as adsorption and desorption, dissolution, redox, etc. In addition, it also includes biological action, including biodegradation and biotransformation. Therefore, we will simplify the methane gas transport and emission model after the degradation of permafrost regions, only considering the main movement process and external influencing factors, as shown in Figure 5.

The top layer area A of the physical model is the active layer and snow cover layer of the permafrost region, which experiences melting in summer and freezing in winter. Area B is the overlying layer after the gradual degradation of the permafrost layer. This part of the area can be simplified as an ordinary porous medium. Methane gas formed by methane hydrate decomposition gradually moves upward through this area. Area C is the porous medium layer containing methane hydrate after the permafrost layer gradually degenerates. The methane hydrate stored in this part of the area will decompose into a large amount of methane gas after the external heat flow enters, thus forming the initial

methane concentration field. The specific physical model parameters are shown in Table 1.

Due to the impact of global warming in permafrost regions, the phase changes after the degradation of the permafrost layer will exacerbate the heterogeneity of the overlying layer, and the rapid migration of gases will also form high-permeability transport channels. The permeability of this part of the migration channel is much higher than that of ordinary permeability areas, which further accelerates the migration of methane gas into the atmosphere. Therefore, we set up three high-permeability channels in the overlying layer model area, with a permeability of $5.7\times10^{13}m^2$ in the ordinary area. High-permeability channel 1 has a permeability of $10.7\times10^{-13}m^2$, high-permeability channel 2 has a permeability of $15.7\times10^{-13}m^2$, high-permeability channel 3 has a permeability of $20.7\times10^{-13}m^2$.

Table S1. Model parameters.

Parameter	Value	Parameter	Value
Thickness of A h_a (m)	3	Poisson's ratio μ	0.3
Width of A d_a (m)	20	Young's modulus E_p (Pa)	4.845×10^9
Thickness of B h_b (m)	20	Permeability K_p (m^2)	5.7×10^{-12}
Width of B d_b (m)	20	Gas composition	100%CH_4
Thickness of C h_c (m)	20	Upper layer porosity n_p	0.38
Width of C d_c (m)	20	Upper layer density ρ_p (kg/m^3)	2600
Density of methane clathrate ρ_h (kg/m^3)	960	Heat transfer coefficient of saturated porous medium k_{p1} (W/(m • K))	3.1
Gas diffusion coefficientD_g (m^2/s)	3.7×10^{-10}	Dry porous medium heat transfer coefficient k_{p2} (W/(m • K))	0.53

From Figure 12 and 13 in the manuscript, it can be seen that within the same migration time, the methane gas concentration in the ordinary permeability region is lower, while the methane gas concentration in the high permeability channel region is higher. As the permeability of the high-permeability channel increases, the methane gas migration speed gradually accelerates, and the methane concentration increases within the same migration time.

In summary, it can be seen that the high-permeability gas channels formed by factors such as the gradual degradation of permafrost layers and gas migration are crucial for the release of methane gas in permafrost regions and cannot be ignored.